Optical and Acoustical Dynamics of Microbubble Contrast Agents inside Neutrophils

Paul A. Dayton,* James E. Chomas,* Aaron F. H. Lum,* John S. Allen,* Jonathan R. Lindner,† Scott I. Simon,* and Kathy W. Ferrara*

*Biomedical Engineering Division, University of California, Davis, Davis, California 95616, and †Cardiovascular Division, University of Virginia, Charlottesville, Virginia 22903 USA

ABSTRACT Acoustically active microbubbles are used for contrast-enhanced ultrasound assessment of organ perfusion. In regions of inflammation, contrast agents are captured and phagocytosed by activated neutrophils adherent to the venular wall. Using direct optical observation with a high-speed camera and acoustical interrogation of individual bubbles and cells, we assessed the physical and acoustical responses of both phagocytosed and free microbubbles. Optical analysis of bubble radial oscillations during insonation demonstrated that phagocytosed microbubbles experience viscous damping within the cytoplasm and yet remain acoustically active and capable of large volumetric oscillations during an acoustic pulse. Fitting a modified version of the Rayleigh-Plesset equation that describes mechanical properties of thin shells to optical radius-time data of oscillating bubbles provided estimates of the apparent viscosity of the intracellular medium. Phagocytosed microbubbles experienced a viscous damping approximately sevenfold greater than free microbubbles. Acoustical comparison between free and phagocytosed microbubbles indicated that phagocytosed microbubbles produce an echo with a higher mean frequency than free microbubbles in response to a rarefaction-first single-cycle pulse. Moreover, this frequency increase is predicted using the modified Rayleigh-Plesset equation. We conclude that contrast-enhanced ultrasound can detect distinct acoustic signals from microbubbles inside of neutrophils and may provide a unique tool to identify activated neutrophils at sites of inflammation.

INTRODUCTION

Ultrasound contrast agents are microbubbles composed of a thin lipid or albumin shell filled with air or a high-molecular-weight gas. When these microbubbles are subjected to an acoustic pulse produced by an ultrasound transducer, the pressure wave causes the bubbles to undergo volumetric oscillations that subsequently produce a secondary acoustic pulse detectable by the imaging system. This acoustic property makes microbubbles highly detectable with a clinical ultrasound system. Typically, the acoustic echo from blood is 30–40 dB less than that from tissue, but the presence of ultrasound contrast agents provides a significant increase in the echo amplitude from blood-filled regions, thereby enabling the measurement of tissue blood perfusion. Ultrasound contrast agents have been shown to be particularly useful in the assessment of myocardial tissue perfusion in cardiology (Wei and Kaul, 1997).

More recently, it has been demonstrated that microbubbles attach to and are phagocytosed by activated leukocytes (Lindner et al., 2000). Activated leukocytes become adherent to the endothelium of post-capillary venules during the inflammatory responses triggered by infection, injury, or ischemia-reperfusion (Ley, 1996). The extent of microbubble attachment appears to directly correlate with the degree of inflammation (Lindner et al., 2000). In these studies, the viability of leukocytes was not observed to be affected by microbubble phagocytosis. Exploiting these binding and targeting properties of leukocytes, ultrasound imaging of phagocytosed microbubbles may be applied to gauge the spatial extent and severity of inflammation. Currently, the only technique that is available for this application is single-photon emission computed tomography (SPECT) with radiolabeled leukocytes. Isotopes of technitium or indium are used to label leukocytes and assess their recruitment during inflammatory diseases, sepsis, osteomyolitis, and myocardial infarction (Gainey et al., 1988; Roddie et al., 1988; Thakur et al., 1977). Use of this technique is limited due to the poor spatial resolution of SPECT (on the order of 2 mm), the complications of working with radioisotopes, and the high cost and limited availability of SPECT cameras. These shortcomings highlight the need to develop an approach for the diagnosis of inflammatory diseases with ultrasound imaging.

Pulse-inversion imaging is a method for the detection of contrast agent microbubbles. This technique relies on transmitting a pair of acoustic pulses of opposite phase and then summing the received signal. The echoes from linear scatterers such as tissue at low acoustic pressures cancel during summation, whereas microbubbles that are nonlinear scatterers emit echoes that sum coherently. This technique has shown increased imaging contrast compared with conventional microbubble-detection techniques, but suffers from the fact that at higher acoustic pressures, propagation of the transmitted pulse through tissue produces confounding nonlinear pulse distortion. The result is that for the higher acoustic pressures often used in clinical imaging, nonlinear echoes from tissue are detected along with the echoes from microbubbles, resulting in

Received for publication 1 June 2000 and in final form 12 December 2000.

Address reprint requests to Dr. Katherine Ferrara, Department of Biomedical Engineering, 1 Shields Avenue, University of California, Davis, Davis, CA 95616-5294. Tel.: 530-754-9436; Fax: 530-752-7156; E-mail: kwferrar@ucdavis.edu.

0006-3495/01/03/1547/10 $2.00

degraded image quality. A second strategy for the discrimination of microbubbles using phase-inverted acoustic pulses involves detection of the frequency difference (termed the frequency shift) between bubble echoes that result from transmission of pulses with a different phase. This method is based on the observation that bubbles produce a higher mean frequency echo in response to a one-cycle rarefaction-first pulse than to a compression-first pulse. Tissue does not elicit this same phase-specific frequency shift. The frequency difference provides an additional characteristic with which the signal from bubbles can be differentiated from the signal from tissue (Morgan et al., 2000).

For contrast agent microbubbles to be echogenic, they must be able to oscillate to an extent that produces a detectable acoustic pulse or signature. Currently, the effect of phagocytosis on the oscillatory response of microbubble contrast agents during insonation is unknown. The objective of the current study is to analyze the physical effects of neutrophil phagocytosis on microbubble oscillation and determine whether free and phagocytosed microbubbles can be differentiated acoustically. Our experimental strategy uses a high-speed imaging system to visualize microbubble oscillations during insonation. Acoustic echoes from individual free and phagocytosed microbubbles are recorded in response to a phase-inversion pulsing scheme. A comparison of radial dynamics observed for free and phagocytosed microbubbles shows significant intracellular damping. Predictions from a modified Rayleigh-Plesset equation corroborate differences in oscillation observed experimentally and provide a unique means of estimating viscoelastic properties of neutrophils. The data show that microbubbles oscillate differently within neutrophils and emit acoustic signals that are distinct from free microbubbles.

ANALYSIS

Simulation of bubble oscillation and estimation of viscosity

When an ultrasound contrast microbubble is insonified with an acoustic pulse, the bubble oscillates and produces an acoustic signature, which can then be detected with an imaging system. To corroborate the validity of our results, and to predict values for neutrophil viscoelastic damping, a theoretical model was used to simulate contrast microbubble response during insonation (Eq. 1). Notation and constants used in the evaluation of Eq. 1 are listed in Tables 1 and 2. This model differs from the Rayleigh-Plesset equation in that it incorporates radiation losses into the surrounding fluid in addition to the inclusion of additional terms for viscosity and elasticity of the shell.

$$\rho R\ddot{R} + \frac{3}{2}\rho\dot{R}^2 = \left(P_o + \frac{2\sigma}{R_o} + \frac{2\chi}{R_o}\right)\left(\frac{R_o}{R}\right)^{3\gamma}\left(1 - \frac{3\gamma}{c}\dot{R}\right) - \frac{4\mu\dot{R}}{R} - \frac{2\sigma}{R}\left(1 - \frac{1}{c}\dot{R}\right) - \frac{2\chi}{R}\left(\frac{R_o}{R}\right)^2\left(1 - \frac{3}{c}\dot{R}\right) - 12\mu_{sh}\varepsilon\frac{\dot{R}}{R(R-\varepsilon)} - (P_o + P_{driv}(t)) \quad (1)$$

TABLE 1 Notation

Symbol	Definition
c	Speed of sound in liquid
P	Time-dependent pressure
$P_{driv}(t)$	Time-varying acoustic pressure
P_o	Hydrostatic pressure
R	Instantaneous bubble radius
$\dot{R}$	Velocity of bubble wall
$\ddot{R}$	Acceleration of bubble wall
R_o	Initial bubble radius
χ	Elasticity modulus of lipid shell
ε	Thickness of lipid shell
ρ	Liquid density
μ	Cytoplasmic viscosity
μ_{sh}	Viscosity of lipid shell
σ	Surface tension coefficient
γ	Polytropic gas exponent

The left-hand side of the equation represents the inertial terms of the Rayleigh-Plesset equation. The first term on the right-hand side represents the pressure within the gas, the second term represents the effect of the cell viscosity, the third term represents the effect of interfacial tension, the fourth term the effect of shell elasticity, the fifth term the effect of the shell viscosity, and the final terms indicate the driving acoustic pressure relative to the pressure at an infinite distance from the microbubble. The values for the shell parameters, χ (elasticity modulus) and $\mu_{sh\epsilon}$ (product of shell thickness and viscosity of thin shell) were previously determined from optical radius-time curves for free microbubbles recorded for a range of driving pressures (100–400 kPa), pulse lengths (one-, two-, three-, and seven-cycle transducer excitations), and two different phases (Morgan et al., 2000). The term $2\sigma/R$ is a composite interfacial tension representing the sum of the gas-lipid and the lipid-water tensions. We use 0.051 N/m as the estimated sum of these coefficients. During insonation and bubble expansion, the interfacial tension is expected to change dynamically as air diffuses into the decafluorobutane gas core and as the lipid shell cracks. Such cracks expose the gas core directly to the water, with a resulting maximum interfacial tension of 73 mN/m for an air/water interface. Although the exact value for this surface tension is unknown and time varying, the predicted microbubble radial expansion over a range of σ from 20–73 mN/m differs by a maximum of ~6%. Thus, the magnitude of the surface tension has a small effect on the predicted oscillatory behavior. Estimates of intracellular viscosity μ were produced by fitting radius-time curves predicted by the model to radius-time curves optically recorded from phagocytosed microbubbles with a high-speed camera as described in Materials and Methods. The minimum mean square error between predicted and experimental radius-time curves was calculated for a range of viscosities from 1 to 30 cp. Intracellular viscosity was predicted by minimizing the mean square error (z) over the viscosity parameter μ between the simulation (x) and the optical data (y). The driving pressure waveform

TABLE 2 Parameters used in evaluation of model

Parameter	Value
c	1540 m/s
P_o	101 kPa
χ	0.26 N/m
ρ	998 kg/m^3
σ	0.051 N/m
$\mu_{sh}\varepsilon$	(1.49R_o − 0.86) nm Pa s (R_o in μm)
γ	1.07

for the model was produced directly from acoustic hydrophone measurements. Mean square error was calculated as

$$z^2 = \frac{1/2[\overline{((x-\bar{x})-(y-\bar{y}))^2}]}{\overline{(x-\bar{x})^2+(y-\bar{y})^2}}. \quad (2)$$

Predictions for the microbubble echo

Predictions for free and phagocytosed microbubble echoes are also produced by this model. The echo produced by the microbubble is approximated by Eq. 3 (Leighton, 1994), where $\ddot{R}$, $\dot{R}$, and R are determined from Eq. 1 by solving the differential equation for the pressure in the liquid, P.

$$P = \rho r^{-1}(R^2\ddot{R} + 2R\dot{R}^2) \quad (3)$$

Thus, the experimental and predicted echoes are compared directly.

Calculation of echo mean frequency

For both predicted and experimentally acquired echoes, the mean frequency (f_{mean}) of bubble echoes was calculated using

$$f_{mean} = \frac{\sum_{f=0}^{10} f \times S(f)}{\sum_{f=0}^{10} S(f)}. \quad (4)$$

This relation was also used to approximate the mean frequency of oscillation for optical radius-time curves. In this relation, f is the spectral frequency bin, and $S(f)$ is the amplitude of the Fourier transform of the echo or radius-time curve at each bin.

Statistical analysis

The Student's t-test was used to evaluate statistical significance between variables. Nonparametric comparisons employed a Wilcoxon rank-sum test. Comparisons between mean values were considered to be statistically significant at $p \leq 0.05$.

MATERIALS AND METHODS

Cell preparation

Whole blood was collected from healthy volunteers into a heparinized syringe (10 U/mL) using the human subject protocol approved by the Human Subjects Review Committee at the University of California, Davis. Plasma was obtained by centrifugation at 400 × g. Neutrophils were isolated using Ficoll-Hypaque density gradient centrifugation (Mono-Poly, ICN Pharmaceuticals, Costa Mesa, CA) and washed with 25 ml of a HEPES buffer (30 mM HEPES, 110 mM NaCl, 10 mM KCl, 1 mM $MgCl_2$, 10 mM glucose) and human serum albumin (0.1%). Cells were resuspended in 500 μl of the HEPES buffer at 2×10^7 cells/ml. Microbubbles consisted of an experimental phospholipid-shelled contrast agent with a decafluorobutane core (MP1950, Mallinckrodt, St. Louis, MO). Although the term encapsulated gas microparticles more accurately describes these contrast agents, they are called microbubbles in medical ultrasound and are thus denoted as such in this work. To promote neutrophil capture and phagocytosis, microbubbles were opsonized by addition of autologous plasma at a 1:8 volume ratio for 15 min at 37°C. Before the experiment, 5×10^5 neutrophils in 160 μl of HEPES buffer (with the addition of 1.5 μM $CaCl_2$) were stimulated with 10 nM formyl peptide and then mixed with 30 μl of the microbubble/plasma solution. The cell-microbubble suspension was mixed continuously in a rotary shaker at 37°C. Phagocytosis of microbubbles was confirmed by optical and electron microscopy.

Electron microscopy of neutrophils and microbubbles

Following preparation of neutrophils and microbubbles as described above, neutrophils were post-fixed by suspending in a 2% glutaraldehyde solution overnight. Samples were then fixed in 2% buffered OsO_4 and dehydrated in steps with ethyl alcohol. Spurrs Resin was used as the embedding media. A transmission electron microscope (H-600, Hitachi, Tokyo, Japan) was used to image neutrophils and microbubbles at ~10,000× magnification.

Radial dynamics measured by high-speed imaging

Optical studies of the effects of ultrasound on phagocytosed microbubbles were performed using two techniques, both of which allow us to observe the radial oscillations of individual phagocytosed microbubbles during insonation. The first system consists of an ultra-high-speed camera (Imacon 468, DRS Hadland, Cupertino, CA) coupled with an inverted microscope (IX-70, Olympus, Melville, NY). The Imacon camera is capable of recording seven sequential image frames at up to 100 million frames per second while simultaneously recording a streak image with 10-ns time resolution. The streak image consists of 576 time samples along a single line of sight at a rate of up to 100 MHz and is sufficiently fast to record the diameter-time curves of insonified microbubbles oscillating at several MHz. Frame images are used to determine whether the bubble or neutrophil is intact. In a second experimental system, a Kodak Motioncorder Analyzer coupled with a pulsed copper-vapor laser (CU-10, Oxford Lasers, Oxford, UK) provided additional images of microbubbles and neutrophils during insonation. The laser-illuminated imaging system provided higher optical resolution than the Imacon camera system. However, it was incapable of the MHz frame rate necessary to produce radius-time curves of oscillating microbubbles. An arbitrary waveform generator (AWG 2021, Tektronix, Wilsonville, OR) was used to produce the transducer excitation. For these studies, the transducer excitation was either a one- or three-cycle sinusoid, with rarefaction preceding compression. Transmission pulses were amplified with an RF amplifier (3200L, ENI, Rochester, NY). A focused 2.25-MHz single-element transducer (V305, Panametrics, Waltham, MA) was positioned in the media adjacent to the sample and provided the ultrasound source. Table 3 provides characteristics for the transducers used in the experimental systems. A calibrated needle hydrophone (PZT 2422–0200, Specialty Engineering Associates, Soquel, CA) was used for acoustic pressure measurements (peak negative pressure), which were made at the focal plane and recorded before each experiment. A custom flow chamber consisting of an optically and acoustically transparent 200-μm cellulose tube, permitted optical observation of the sample during simultaneous insonation. Optical measurements were calibrated with a 10-μm reticle slide indicating resolution on the order of 0.5 μm.

A microinjector (IM-5B, Narishige, East Meadow, NY) hydrostatically coupled to the flow chamber was used to control flow and deliver individual neutrophils that had phagocytosed microbubbles, or free microbubbles, into the sample volume and field of view. The sample volume consisted of the section of the cellulose tube that was positioned at the mutual focus of the transducer and the microscope objective. For optical experiments, the transducer and objective were oriented perpendicular to

TABLE 3 Transducer characteristics

	Transmit (V305)	Receive (V309)
Nominal frequency (MHz)	2.25	5.0
Element diameter (inches)	0.75	0.5
Focal length (inches)	2.32	2.24
Center frequency (MHz)	2.45	5.63
-6-dB bandwidth	75.9%	88%

the cellulose tube. Optical radius-time curves were recorded with the Imacon camera and then digitized off-line using National Institutes of Health image analysis software (National Institutes of Health, Bethesda, MD) and Photoshop (Adobe, San Jose, CA). Off-line measurement, analysis, and modeling were then performed with MATLAB (Mathworks, Natick, MA).

Acoustical dynamics of microbubbles

For acoustical observations, a second experimental system was created that permitted the acquisition of bubble echoes with nearly simultaneous optical observation. An IV-500L microscope (Mikron Instruments, San Diego, CA) was used to optically confirm the presence of a single bubble or cell in the acoustic sample volume. Optical observation was also used to confirm bubble phagocytosis and measure bubble size. The microscope objective was removed ~1 s before acoustic interrogation so as not to interfere with the acoustic signal. Echoes were received with a 5-MHz (V309, Panametrics) transducer oriented perpendicular to the 2.25-MHz transmission transducer. Received signals were amplified with a BR640 receiver (Ritec, Warwick, RI) and digitized with a 9310 digital oscilloscope (LeCroy, Chestnut Ridge, NY). Digitized echoes were processed in MATLAB. A phase-inversion pulse sequence consisting of two single-cycle pulses of opposite phase was used for insonation of microbubbles. The first pulse induced the pressure rarefaction first, and the second pulse induced the pressure compression first.

RESULTS

Neutrophil phagocytosis of opsonized microbubbles

Microbubble contrast agents introduced into the circulation have been reported to preferentially adhere at sites of tissue inflammation (Lindner et al., 2000). Neutrophil adhesion to microbubbles has been shown to depend on plasma complement protein adsorption on the bubble surface and recognition by activated β_2-integrin adhesion receptors on the neutrophil (Lindner et al., 2000). In the current study, human neutrophils were isolated from blood, exposed to a chemotactic stimulus, and then sheared in suspension with opsonized microbubbles to simulate the in vivo process. A sample of this suspension was rapidly fixed in glutaraldehyde and prepared for transmission electron microscopy. The micrographs shown in Fig. 1 depict neutrophils stimulated with formyl peptide and sheared with microbubbles that were or were not opsonized. Neutrophils were observed to undergo shape change and exhibit small pseudopods in response to chemotactic stimulus, but did not phagocytose microbubbles without prior opsonization (Fig. 1 *A*). The majority of neutrophils sheared with opsonized microbubbles were observed to have phagocytosed at least one and often several microbubbles (Fig. 1 *B*). Microbubbles inside of cells were surrounded by a tightly apposed phagosomal membrane as has been previously described for opsonized latex microspheres (Simon and Schmid-Schonbein, 1988). In these cells, there was no indication of cell sphering due to excess fluid uptake as evidenced by a similar granule density and excess membrane surface area compared with control neutrophils. For the acoustic experiments, neutrophils and microbubbles were observed in the cellulose tube under the light microscope. By incrementing the flow with the microinjector it was possible to measure the diameter of each microbubble and confirm for each neutrophil that a single microbubble was phagocytosed before insonation.

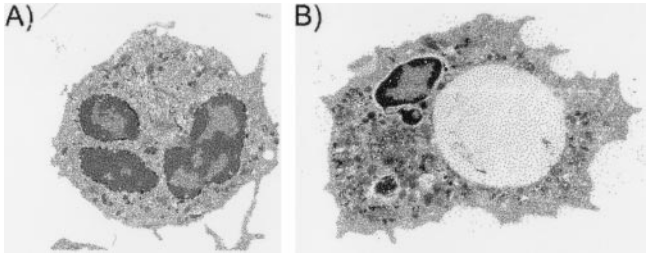

FIGURE 1 Electron micrographs of neutrophils stimulated with formyl peptide. Cells were sheared with microbubbles that were not (*A*) and were (*B*) opsonized. The neutrophil in *B* has phagocytosed a large (~2.5 μm) microbubble. Although neutrophils were not observed to phagocytose non-opsonized microbubbles, the majority of neutrophils sheared with opsonized microbubbles phagocytosed one or several microbubbles.

Radial dynamics of microbubbles

Radius-time curves for free and phagocytosed microbubbles during insonation were compared to determine the effects of the intracellular environment on bubble oscillation. The radius-time curves were acquired in the form of streak images, which are optical recordings of a single line-of-sight over time using a high-speed camera. With the line-of-sight along the center of the bubble, the resulting image is a space-time recording of the oscillations of the insonified bubble. The streak is recorded over a 5-μs time interval, with a time resolution of 10 ns.

Such an image of a 1.5-μm radius bubble during insonation reveals bubble oscillations in response to a one-cycle rarefaction-first 2.25-MHz pulse at an acoustic pressure of 600 kPa (Fig. 2 *A*). In this example, a microbubble is observed to expand to a maximum of 333% of its initial

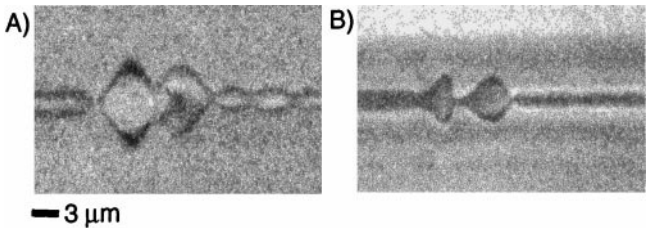

FIGURE 2 Streak images of microbubbles revealing oscillations in bubble diameter over a 5-μs time period during acoustic interrogation. Both images show 1-μm-radius bubbles oscillating in response to a rarefaction-first, 1-cycle, 600-kPa acoustic pulse. (*A*) Oscillations of a free microbubble; (*B*) oscillations of a microbubble within a neutrophil illustrating the damping due to the increased density of the surrounding cellular milieu.

radius in response to pressure rarefaction. A streak image acquired with a 1.5-μm-radius bubble inside of a neutrophil illustrates a phagocytosed microbubble that expands to 233% under the same insonation conditions (Fig. 2 *B*). Also note the differences in damping between Fig. 2, *A* and *B*. The oscillation of the bubble within the leukocyte is shown to end abruptly.

The digitized radius-time curves for the examples presented in Fig. 2, *A* and *B*, are shown in Fig. 3. The first minima of the echo waveforms at 0.7 s have been aligned to highlight the difference between the frequency response of the free and phagocytosed microbubbles. For the free microbubble the duration of the first cycle is 0.57 μs, compared with 0.41 μs for the phagocytosed microbubble, indicating that the phagocytosed microbubble oscillates at a higher frequency than the free microbubble.

The mean frequency of oscillation was calculated from optical data for radius-time curves of free and phagocytosed microbubbles of similar radius ($\sim$1.5 μm) insonified with a one-cycle rarefaction-first pulse at 600 kPa. The phagocytosed microbubbles ($N = 4$) oscillated at a frequency of $\sim$150 kHz higher ($p < 0.05$) than the free microbubbles ($N = 5$). The ratio of the maximum of the first expansion to the initial radius was recorded from digitized radius-time curves for both free and phagocytosed microbubbles. Table 4 illustrates the differences in the expansion ratio for free and phagocytosed bubbles of similar radius. Data show that phagocytosed microbubbles expand less than free microbubbles, indicating a damping effect of the intracellular environment. Bubble oscillation over longer pulse lengths did not show a significant difference in maximum expansion for free and phagocytosed microbubbles.

We have also observed that the expansion of phagocytosed microbubbles increased with increasing acoustic pressure. At low to moderate acoustic pressures ($<$1 MPa), the bubble expansion during pressure rarefaction did not cause cell lysis. However, as peak acoustic pressure was increased above 1 MPa, bubble expansion occupied a significant fraction of cell volume, often resulting in cell lysis. Expansion of a microbubble within a neutrophil is demonstrated in Fig. 4, where six frames selected from two sequences show neutrophils that have phagocytosed 1.5-μm-radius microbubbles. Observation of bubble dynamics in response to a 900-kPa acoustic pulse reveals that the bubble expands to a large fraction of the neutrophil volume in a reversible process without causing membrane rupture (Fig. 4, *A–C*). The frames show the bubble before insonation, during peak expansion (pressure rarefaction), and after insonation. At peak expansion, the cell membrane appears stretched taut over the spherical shell. In the next three frames, a 1.6-MPa acoustic pulse causes a bubble to expand to such a large extent that the neutrophil lyses, releasing its contents into the surrounding medium (Fig. 4. *D–F*). Frames *A–C* were recorded with the Imacon high-speed camera and hence appear to be of different quality than *D–F*, which were recorded with the laser-based imaging system.

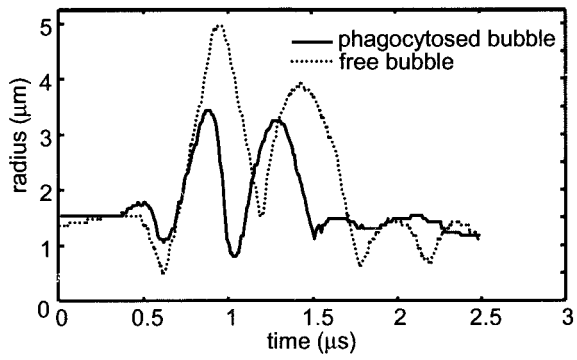

FIGURE 3 Radius-time curves for free and phagocytosed microbubbles measured from streak images. The acoustic pulse has rarefaction first with a peak pressure of 600 kPa. The dotted line shows the radius of the free microbubble, and the solid line shows the radius of the phagocytosed microbubble. The free microbubble oscillates with a lower mean frequency and larger radial displacement than the phagocytosed microbubble.

Simulations of microbubble dynamics

To determine values of neutrophil apparent viscosity that correspond to the optically recorded radius-time oscillations, a numerical evaluation of Eq. 1 was conducted, varying μ from 1 to 30 cps. The best fit was determined by minimizing the mean square error for each radius-time curve (Eq. 2). Estimates of viscosity for phagocytosed and free microbubbles as determined by this method are presented in Table 5, which indicates that the mean viscosity of the neutrophil is 12 cps, compared with 1.7 cps estimated for the saline buffer. The predicted radius-time curves accurately match the measured frequency and amplitude of oscillation. For 29 observations, the normalized mean square error for these curves was 0.26 for phagocytosed bubbles and 0.37 for free bubbles. An example of a predicted radius-time curve overlaid on experimental data is shown in Fig. 5. For this case, an apparent viscosity of $\sim$11 cps provided the minimum mean square error and best radius-time curve fit.

Acoustic observations

We next examined the acoustic echoes for both free and phagocytosed microbubbles. The resting radius of each microbubble was measured from the video record $\sim$1 s before insonation. The transmitted center frequency was 2.25 MHz and the peak negative pressure was 600 kPa. A transmitted pulse sequence consisting of a one-cycle rarefaction-first pulse followed by a one-cycle compression-first pulse was used to insonify the microbubbles. Both free and phagocytosed microbubbles produce a similar echo waveform for the compression-first pulse. In contrast, during the rarefac-

TABLE 4 Comparison of expansion of free and phagocytosed microbubbles from optical data

Microbubble	Cycles/pressure (kPa)	N	Mean radius (μm)	Maximum expansion ratio	Statistical significance from phagocytosed microbubble
Free	1st cycle 300	5	1.4	173%	$p < 0.05$
Free	1st cycle 600	11	1.5	272%	$p < 0.05$
Phagocytosed	1st cycle 300	4	1.4	153%	
Phagocytosed	1st cycle 600	13	1.5	227%	

Measurements of maximum expansion ratio (maximum diameter of first cycle to initial diameter) for free and phagocytosed microbubbles demonstrating that phagocytosed microbubbles expand less than free microbubbles in response to an acoustic pulse of the same intensity.

tion-first pulse, phagocytosed microbubbles were found to oscillate with a higher frequency than free bubbles, which was consistent with the optical radius-time data. Recorded echoes presented in Fig. 6 demonstrate that free and phagocytosed microbubbles of ~1.5-μm radius produce echoes with the same mean frequency for the compression-first pulse (3.4 MHz). For the free microbubble, the mean frequency of the rarefaction-first echo is also 3.4 MHz, in contrast to the echo from the rarefaction-first pulse for the phagocytosed bubble, which has a significantly higher mean frequency of 4.2 MHz.

The frequency shift is the difference between the frequency of the rarefaction-first pulse and that of the compression-first pulse. The mean frequency shift for phagocytosed microbubbles was consistently higher than for free microbubbles of the same radius. The frequency shift is compared for free and phagocytosed microbubble echoes in Table 6.

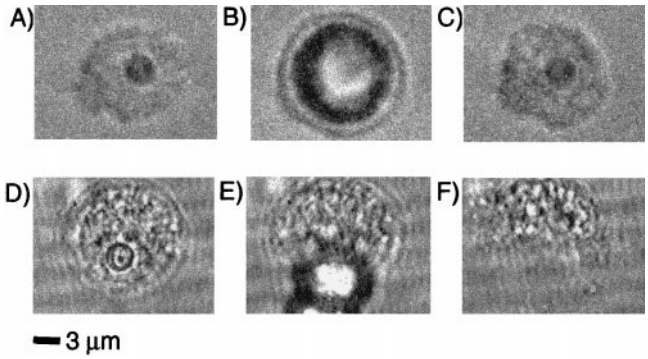

FIGURE 4 Individual neutrophils with phagocytosed microbubbles insonified at moderate (*A–C*) and high (*D–F*) acoustic pressures. Frames *A* and *D* show the phagocytosed microbubble before insonation. In *B* the bubble expands during the pressure rarefaction of 900 kPa. (*C*) The bubble after expansion with moderate pressure insonation, and with the neutrophil intact. (*E*) The microbubble during the pressure rarefaction of 1.6 MPa, during which the bubble expands beyond the limits of the neutrophil membrane. The lysed neutrophil is all that remains in *F*. The first three images were acquired with the high-speed Imacon camera system with a 50-ns shutter speed. The second three images were taken with a digital camera illuminated by a 30-ns pulsed laser. The frame rate of the Imacon camera is higher than the laser-illuminated system; however, higher spatial resolution is obtained with the laser system.

Simulation of acoustic echoes from microbubbles

In this section, predicted echoes are calculated based on Eqs. 1 and 3 and compared with those recorded in acoustic experiments. The echoes recorded acoustically from phagocytosed microbubbles have a higher mean frequency when insonified with a rarefaction-first pulse as compared with a compression-first pulse, with a shift in mean frequency of 0.61 MHz reported in the previous section (Table 6).

We examined whether microbubble echoes calculated from the predicted radius-time curves and Eq. 3 would demonstrate the large frequency shift measured experimentally. Frequency shifts were calculated from the simulated echoes as a function of bubble radius and cell viscosity. The insonation pulse sequence consisted of a rarefaction-first pulse followed by a compression-first pulse. Simulated frequency shifts (MHz) for bubbles of 1.5- and 2-μm radii and several values of media viscosity are listed in Table 7.

The calculated frequency shift from Eqs. 1 and 3 was observed to increase with an increasing cellular viscosity parameter to a maximum value. The acoustic echoes obtained in the experiments similarly indicate that phagocytosed microbubbles produce a larger frequency shift than free microbubbles, likely due to this larger viscosity. It was also observed that for larger bubbles the frequency shift was smaller. These results are in agreement with experimental observations.

DISCUSSION

Microbubble contrast agents have previously been shown to become phagocytosed intact within minutes of adhesion by activated leukocytes (Lindner et al., 2000). Electron microscopy confirmed that microbubbles were indeed phagocy-

TABLE 5 Viscosity estimates

Microbubble	N	Mean radius (μm)	Viscosity (cps)
Free	15	1.8 ± 0.4	1.7 ± 1.6
Phagocytosed	14	1.4 ± 0.3	12 ± 5.2

Viscosity estimates determined from fitting the theoretical model to experimental data by varying the medium viscosity indicate that microbubbles experience a viscosity approximately sevenfold greater within a neutrophil than in water ($p < 0.05$).

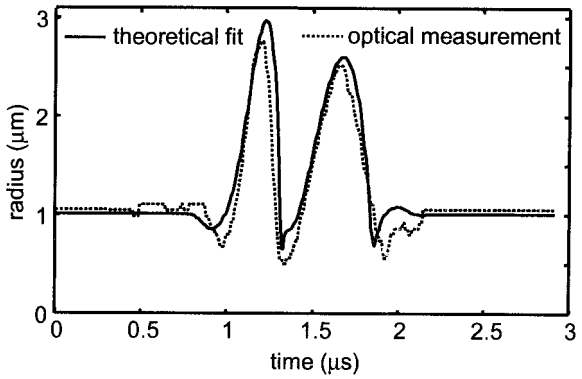

FIGURE 5 Comparison between experimentally recorded radius-time curves with theoretical predictions for a microbubble of 1 μm radius insonified with a rarefaction-first pulse of 600 kPa. For this example, the best fit to the experimental data provided an 11-cps estimate of cytoplasmic viscosity.

tosed and surrounded tightly by a phagosomal membrane such that the bubble shell coupled directly to the cell interior. Furthermore, these leukocytes adhere in regions of inflammation in vivo and can be detected by clinical ultrasound provided that freely circulating microbubbles are cleared from the blood pool (Lindner et al., 2000). In the current study, human neutrophils were stimulated to phagocytose microbubble contrast agents. The physical properties of phagocytosed microbubbles were compared with free microbubbles in suspension. We provide optical verification that microbubbles oscillate differently when inside neutrophils in response to insonation and emit acoustic signals that are distinct from free microbubbles. Optical and acoustical observations of microbubbles agree with numerical predictions based on lipid shell dynamics as predicted by a modified Rayleigh-Plesset equation. A value for intracellular viscosity was found that is consistent with current rheological models of neutrophils.

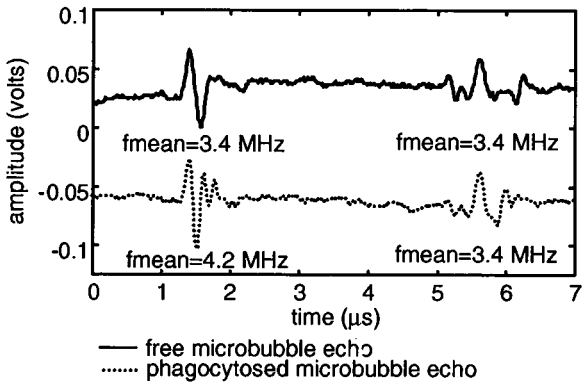

FIGURE 6 Echo signature of similarly sized free and phagocytosed microbubbles in response to two single-cycle pulses of opposite phase and peak pressure of 600 kPa. The first echo is in response to a rarefaction-first pulse; the second is in response to a compression-first pulse. The beginning of the first cycles have been aligned to illustrate the higher frequency content in the phagocytosed microbubble echo. Although both bubbles exhibit similar echo features for the compression-first pulse, the phagocytosed microbubble oscillates at a higher frequency than the free microbubble in response to the rarefaction-first pulse.

TABLE 6 Frequency shift measurements

Microbubble	N	Mean radius (μm)	Mean shift (MHz)
Free	16	1.5 ± 0.1	0.09 ± 0.3
Phagocytosed	25	1.4 ± 0.2	0.70 ± 0.2

Received echoes demonstrate that phagocytosed microbubbles produce a significantly higher frequency shift than free microbubbles for the same bubble size ($p < 0.05$).

Microbubble dynamics in response to insonation

Microbubbles were directly observed by light microscopy and their oscillation during insonation was recorded with a high-speed camera with 10-ns time resolution. The results were compared with echoes obtained by incorporating an acoustical observation system and with those obtained with the numerical predictions.

The range of transmitted pressures used in these experiments correspond well with those available on clinical instruments, and the oscillations of phagocytosed microbubbles vary greatly over this range of pressure. Current clinical ultrasound systems generate an acoustic pressure pulse with a peak negative pressure in the range from 100 kPa to 2.9 MPa over a range of frequencies that include 2.25 MHz. Frequencies between 1 and 2.5 MHz are typically used to image contrast agents and correspond to the resonant frequencies of some agents. Lower transmitted pressures are typically used in continuous imaging modes, and higher pressures are used in a destructive mode in which the agent is intentionally destroyed. Pulse trains that include a range of amplitudes and phase-inverted pulses are under development and are currently being investigated in the clinical setting.

Microbubbles contained within the neutrophil cytoplasm were observed to expand 20–45% less during the first cycle of insonation than free microbubbles. Over longer pulse lengths, the expansion difference was not significant. In response to insonation at moderate acoustic pressures ($\leq$600 kPa) both free and phagocytosed microbubbles were capable of expansion up to 260% of initial diameter. Also,

TABLE 7 Predicted frequency shifts for different medium viscosities

Microbubble radius (μm)	Shift, 1 cps (MHz)	Shift, 6 cps (MHz)	Shift, 11 cps (MHz)
1.5	0.82	1.24	1.10
2.0	0.59	1.00	0.94

Frequency shifts calculated from predicted echoes show higher frequency shifts for bubbles in media of higher viscosity.

for transmitted acoustic pressures less than 600 kPa, compression and expansion of phagocytosed microbubbles occurred without obvious damage to the neutrophil. However, acoustic pressures of 1.6 MPa and higher consistently resulted in expansions that ruptured the neutrophil membrane producing cell lysis.

The radius-time curves observed optically provide direct evidence of the effect of the neutrophil on the microbubble oscillation at low to moderate transmitted intensities. The rate of bubble oscillation in response to a one-cycle rarefaction-first pulse was ~150 kHz higher for phagocytosed microbubbles than that for free microbubbles of similar radius. Eq. 3 specifies the relationship between the radius-time curve R and the predicted echo P, and this relation is in effect a high-pass filter. Thus, the magnitude of the shift in mean frequency for the echo is, as expected, greater than the shift calculated from the radius-time curves. No significant difference in the spectrum of the radius-time curve was observed for higher pressures or longer excitations.

Coupling the acoustical and optical systems allowed digitization of the radio-frequency echoes from individual bubbles with nearly simultaneous optical observation for measurements of bubble size and confirmation of phagocytosis. Acoustic echo signatures obtained from phagocytosed microbubbles were discriminated from free microbubbles in that they exhibited a higher mean frequency in response to a one-cycle rarefaction-first pulse than free microbubbles. There was no significant difference for one-cycle compression-first pulses. For a phase-inversion pulse sequence, the mean frequency shift (difference) between echoes from the two phases was 610 kHz greater for phagocytosed microbubbles than free microbubbles. The echo spectrum is effectively a high-pass filtered version of the spectrum of radial oscillation. Therefore, it is expected that these spectral differences are more prominent in the echo than in the radial oscillation. This frequency difference provides a sensitive means of differentiating the echoes from free and phagocytosed microbubbles of similar size.

Using the optical and acoustical systems, it was verified that echoes from individual microbubbles could be recorded. Discriminating between free and phagocytosed populations of microbubbles is more difficult, however. Using the modified Rayleigh-Plesset equation, Morgan et al. (2000) determined that free lipid-shelled microbubbles with a radius between 1.5 and 2 μm produce a small frequency shift, whereas we have found that the shift produced by phagocytosed bubbles is maximized in this size range. Thus, a bubble population with a consistent diameter in this range would ensure the greatest signal-to-noise ratio. The most significant parameter in the imaging system is the receive bandwidth. A fractional receive bandwidth near 100% is required to detect a frequency shift of several hundred kHz. Systems with this wide bandwidth exist, but are not yet widely available. Increased system bandwidth will improve the signal-to-noise ratio of the technique.

Simulations of radius-time curves using a modified Rayleigh-Plesset equation accurately modeled the oscillation dynamics for both free and phagocytosed microbubbles. Using this equation to optimize a fit to the observed radius-time curves, we predicted a higher mean frequency shift for phagocytosed microbubbles insonified with the phase-inversion pulsing sequence. The magnitude of the frequency shift corroborated with the acoustic measurements of echoes from phagocytosed microbubbles, although the exact values differed from the experimental data by several hundred kHz. Differences may be due to the fact that the predictions for the frequency shift that result from Eqs. 1 and 3 do not account for the inherent low-pass filtering of the echo due to acoustic propagation through the water bath. Note that although this affects the magnitude of the frequency shift for simulated predicted echoes, it does not impact the accuracy of radius-time curves.

Neutrophil rheology affects microbubble behavior

A set of radius-time curves were produced by Eq. 1 with varied values for the cell viscosity (μ), and these curves were fit to experimental data. This produced the estimate of the apparent viscosity of the neutrophil's cytoplasm and organelles surrounding the microbubble. Apparent viscosity was predicted to be ~12 cps, an order of magnitude greater than that of water. Previous measurements of neutrophil viscosity were made by micropipette aspiration of neutrophils in the resting or inactive state (Needham and Hochmuth, 1990; Evans and Yeung, 1989; Tsai et al., 1993). The micropipette technique involves observation of neutrophils as they are aspirated into a micropipette and thus undergo deformation under defined pressures. Estimates of neutrophil viscosity are then derived from a rheological model based on assumptions regarding the nature of the cell membrane together with the cytoskeletal elements, nucleus, and organelles. The rheological behavior of neutrophils undergoing small deformations has been characterized using viscoelastic solid models (Schmid-Schoenbein et al., 1981; Sung et al., 1988). Studies of large deformation and recovery of neutrophils after micropipette aspiration (Evans et al., 1989; Needham et al., 1990) indicate that the plasma membrane and underlying cortical cytoskeleton exert a uniform residual tension on the interior fluid that behaves as a highly viscous non-Newtonian liquid droplet (Evans and Kukan, 1984). Estimates for the cytoplasmic viscosity of passive neutrophils as measured with the micropipette technique has yielded values that range from 1300 to 2000 ps. Recent studies by Tsai et al. (1993) demonstrated a strong dependence of the neutrophil viscosity on the pipette aspiration pressure and resulting shear rate of cytoplasmic flow. Experiments performed at low pressure, corresponding to smaller effective shear rates of flow into the pipette, yielded large estimates of apparent viscosity (~5000 ps). In contrast, when cells were aspirated at 10-fold higher aspiration

pressure they flowed rapidly into the pipette yielding a much lower estimate for viscosity (~500 ps) (Tsai et al., 1993). The difference in shear rate between these experiments is postulated to account for the wide range of measured apparent viscosities, which were measured over a range of shear rates. Tsai et al. (1993) found that the shear rate dependence on viscosity follows a power-law function:

$$\mu = \mu_c \left(\frac{\dot{\gamma}_m}{\dot{\gamma}_c} \right)^{-b} \quad (5)$$

In this case, μ is the apparent cytoplasmic viscosity, $\dot{\gamma}_m$ is the mean shear rate, μ_c is the characteristic viscosity at shear rate $\dot{\gamma}_c$, and b is an exponent characteristic of the material (~0.5 for the passive neutrophil cytosol (Tsai et al., 1993)).

In an attempt to reconcile the relatively low apparent viscosity predicted by the modified Rayleigh-Plesset equation given the measured radius-time curves, we have estimated the shear rates imposed on the cell cytoplasm by the oscillating microbubble. In response to an acoustic pulse with a peak pressure of 900 kPa, we estimate maximum shear rates from $\sim 3.5 \times 10^7$ to $\sim 6 \times 10^7$ for bubble radii between 0.5 and 2.5 μm (not respectively). In this case, the maximum shear rate occurs for bubbles of resonant size at 2.25 MHz, which is close to 1.5 μm. These values are calculated from the change in the velocity of the bubble wall over the radial displacement. Assuming the cell interior is coupled to the microbubble surface and that the cytosol behaves as a power-law fluid, we estimate an apparent viscosity of ~26 cps for the shear rates induced by a 1.5μm bubble during bubble oscillation. With this consideration, the current prediction of ~12 cps fits closely to what is expected at the extremely high shear rates produced during insonation of the microbubble. Shown in Fig. 7 is the current estimate of cytoplasmic viscosity together with those previously published plotted on a logarithmic scale with shear rate. The power-law relation between viscosity and shear appears to reconcile the estimates of apparent viscosity measured over five orders of magnitude of experimental shear rates.

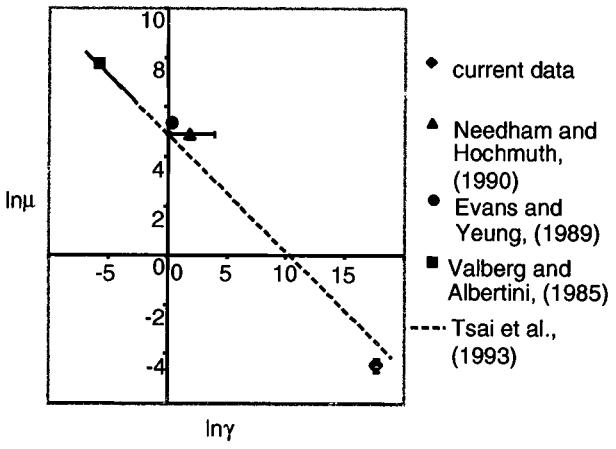

FIGURE 7 Viscosity estimates as a function of shear rate. The estimate of viscosity produced in this paper is compared with estimates of neutrophil viscosity from other laboratories. The dotted line is a fit to the data produced by Tsai et al. (1993) interpolated to the higher shear rates.

In the current model using the Rayleigh-Plesset equation, the cytoplasm is assumed to behave as a Newtonian fluid; therefore, some justification is warranted in regard to the extent to which bubble dynamics deviates from the Newtonian case. A bubble oscillating in a power-law fluid may be expected to experience more damping than in a Newtonian fluid, because radial damping in a power-law fluid follows $|\dot{R}/R|^n$, where n is the material constant (Yang and Yeh, 1966). For $n = 1$, the Newtonian case is recovered. Because we are driving the bubble with very short acoustic pulses (one to three cycles) and at low to medium amplitudes, we assume that significant deviations from the Newtonian case do not develop.

SUMMARY

Combining optical and acoustical experimental systems, we have shown that ultrasound contrast agents phagocytosed by neutrophils oscillate in response to an acoustic stimulus. The observed radial oscillations of phagocytosed microbubbles are accurately predicted by a modified Rayleigh-Plesset equation. This model enabled prediction of the neutrophil cytoplasmic viscosity yielding a mean value that is consistent with values obtained by other laboratories at lower shear rates. This viscosity damped the radial oscillations of phagocytosed microbubbles in comparison with free microbubbles.

The experimental ultrasound system described in this paper was able to detect both free and phagocytosed single microbubbles. The large dynamic range of current clinical systems also provides the opportunity to detect the echo from one microbubble in the presence of tissue and blood echoes. Thus, microbubbles within neutrophils can be detected, providing a potential method to image activated neutrophils as they accumulate at sites of inflammation and ingest microbubbles. Because phagocytosed microbubbles remain acoustically active, contrast agents within neutrophils could be distinguished from tissue, particularly with phase-inversion insonation. Phase-inversion pulsing sequences allow the discrimination of bubbles from tissue by measuring the significantly higher mean frequency shift of the returned echo from contrast agents (Morgan et al., 2000). In particular, the frequency shift produced by free microbubbles is smaller than that produced by phagocytosed microbubbles of the same size, and this difference is sufficient to discriminate free and phagocytosed microbubbles. As shown by other researchers (Morgan et al., 2000), the frequency shift increases with the transmitted pressure up to a maximum shift of ~1 MHz, with a trans-

mitted pressure near 1 MPa. Thus, a transmitted pressure near this maximum is likely to be optimum and unlikely to destroy the surrounding neutrophil. Furthermore, we have demonstrated that a high-intensity ultrasound pulse (>1.5 MPa) can produce a rarefactional pressure that expands microbubbles sufficiently to rupture the neutrophil membrane, resulting in expulsion of the cell contents. This may offer a means to deliver drugs such as antiinflammatory agents at the site of neutrophil recruitment and tissue injury.

We are gratefully appreciative for the assistance of Alexander L. Klibanov in the preparation of the microbubbles. Also, we appreciate the assistance of Dustin Kruse in designing the LabView code to record acoustic data and Donovan May for his assistance with data acquisition. We also thank David Pearson for assisting in the neutrophil preparation.

This portion of K.F.'s research is sponsored by National Institutes of Health grant CA60681. S.I.S. is an Established Investigator of the American Heart Association, and his work is funded by the National Institutes of Health (AI47294).

J.R.L. is supported by National Institutes of Health grant HL03810 and a beginning grant-in-aid from the American Heart Association Mid-Atlantic Affiliate.

REFERENCES

Berne, R., and M. Levy. 1993. Physiology. Mosby-Year Book, St. Louis.

Evans, E., and B. Kukan. 1984. Passive behaviour of granulocytes based on large deformation and recovery after deformation tests. *Blood.* 64: 1028–1035.

Evans, E., and A. Yeung. 1989. Apparent viscosity and cortical tension of blood granulocytes determined by micropipette aspiration. *Biophys. J.* 56:151–160.

Gainey, M. A., J. A. Siegel, E. M. Smergel, and B. J. Jara. 1988. Indium-111-labeled white blood cells: dosimetry in children. *J. Nuclear Med.* 29:689–694.

Leighton, T. G. 1994. The Acoustic Bubble. Academic Press, San Diego.

Ley, K. 1996. Molecular mechanisms of leukocyte recruitment in the inflammatory process. *Cardiovasc. Res.* 32:733–742.

Lindner, J. R., Coggins, M. P., S. Kaul, A. Klibanov, G. Brandenburger, and K. Ley. 2000. Microbubble persistence in the microcirculation during ischemia-reperfusion and inflammation is caused by integrin- and complement-mediated adherence to activated neutrophils. *Circulation.* 101:668–675.

Lindner, J. R., P. A. Dayton, M. P. Coggins, K. Ley, J. Song, K. W. Ferrara, and S. Kaul. 2000. Non-invasive imaging of inflammation by ultrasound detection of phagocytosed microbubbles. *Circulation.* 102: 531–538.

Morgan, K., J. Allen, P. Dayton, J. Chomas, A. Klibanov, and K. Ferrara. 2000. Experimental and theoretical evaluation of microbubble behavior: effect of transmitted phase and bubble size. *IEEE Trans. Ultrason. Ferroelectr. Freq. Contr.* 47:1494–1508.

Needham, D., and R. M. Hochmuth. 1990. Rapid flow of passive neutrophils into a 4 μm pipet and measurement of cytoplasmic viscosity. *J. Biomed. Eng.* 112:269–276.

Roddie, M. E., A. M. Peters, H. J. Danpure, S. Osman, B. L. Henderson, J. P. Lavender, M. J. Carroll, R. D. Neirickx, and J. D. Kelly. 1988. Inflammation: imaging with Tc-99m HMPAO-labeled leukocytes. *Radiology.* 166:767–772.

Schmid-Schoenbein, G. W., K.-L. P. Sung, H. Tozeren, R. Skalak, and S. Chien. 1981. Passive mechanical properties of human leukocytes. *Biophys. J.* 36:243–256.

Simon, S. I., and G. W. Schmid-Schonbein. 1988. Biophysical aspects of microsphere engulfment by human neutrophils. *Biophys. J.* 53:163–173.

Sung, K.-L. P., C. Dong, G. W. Schmid-Schonbein, S. Chien, and R. Skalak. 1988. Leukocyte relaxation properties. *Biophys. J.* 54:331–336.

Thakur, M. L., J. P. Lavender, R. N. Arnot, D. J. Silvester, and A. W. Segal. 1977. Indium-111-labeled autologous leukocytes in man. *J. Nuclear Med.* 18:1014–1021.

Tsai, M. A., R. S. Frank, and R. E. Waugh. 1993. Passive mechanical behavior of human neutrophils: power-law fluid. *Biophys. J.* 65: 2078–2088.

Valberg, P. A., and D. F. Albertini. 1985. Cytoplasmic motions, rheology, and structure probed by a novel magnetic particle method. *J. Cell. Biol.* 101:130–140.

Wei, K., and S. Kaul. 1997. Recent advances in myocardial contrast echocardiography. *Curr. Opin. Cardiol.* 12:539–546.

Yang, W., and H. Yeh. 1966. Theoretical study of bubble dynamics in purely viscous fluids. *Am. Inst. Chem. Eng. J.* 927–931.